PHYSICAL REVIEW B **92**, 041405(R) (2015)

From ripples to spikes: A hydrodynamical mechanism to interpret femtosecond laser-induced self-assembled structures

George D. Tsibidis,[1,*] C. Fotakis,[1,2] and E. Stratakis[1,3,†]

[1]*Institute of Electronic Structure and Laser (IESL), Foundation for Research and Technology (FORTH), N. Plastira 100, Vassilika Vouton, Heraklion 70013, Crete, Greece*

[2]*Physics Department, University of Crete, Heraklion 71409, Crete, Greece*

[3]*Materials Science and Technology Department, University of Crete, 71003 Heraklion, Greece*

(Received 6 September 2014; revised manuscript received 5 June 2015; published 9 July 2015)

Materials irradiated with multiple femtosecond laser pulses in subablation conditions are observed to develop various types of self-assembled morphologies that range from nanoripples to periodic microgrooves and quasiperiodic microspikes. Here, we present a physical scenario that couples electrodynamics, describing surface plasmon excitation, with hydrodynamics, describing Marangoni convection and counter-rolls, to elucidate this important subablation regime of light-matter interaction in which matter is being modified; however, the underlying process is not yet fully understood. The proposed physical mechanism could be generally applicable to practically any conductive material structured by ultrashort laser pulses; therefore it can be useful for the interpretation of further critical aspects of light-matter interaction.

DOI: 10.1103/PhysRevB.92.041405 PACS number(s): 64.70.D−, 52.38.Mf, 78.20.Bh, 78.47.J−

Over the past decades, material processing with femtosecond pulsed lasers has received considerable attention due to its multiple diverse applications ranging from microdevice fabrication to optoelectronics, microfluidics, and biomedicine [1–4]. Direct femtosecond laser surface micro- and nanopatterning has been demonstrated in many types of materials including semiconductors, metals, dielectrics, ceramics, and polymers. Following irradiation with ultrashort pulses, multiphysical phenomena take place [1,5,6] while a plethora of surface structures can be realized. In the case of metallic and semiconducting materials, including silicon (Si) shown in Fig. 1, periodic submicron ripples are formed at low [Figs. 1(a) and 1(b)] microgrooves at intermediate [Figs. 1(c) and 1(d)] [7] and quasiperiodic arrays of microspikes [Figs. 1(e) and 1(f)] [8,9] at high number of pulses (NP). Similar-looking groove- and spiky-like macrostructures can also be found in nature, when large thermal gradients are developed, for example, in the formation of penitentes [10], jetlike features in the oceans [11], and volcano lava laminar flow [12].

To date, there are numerous reports on the mechanism behind morphological changes [13–24] and, more specifically, the formation of *subwavelength*-sized ripples [25–32]. While a thermocapillary mechanism of melt flow due to a temperature gradient has been suggested in previous works [24,33] to describe morphological changes for nanosecond pulses, there is no interpretation of the microgrooves generation (that develop perpendicularly to the ripples and have a substantially *larger* periodicity than the ripples) and transition to spike formation from the viewpoint of physics; furthermore, while the excitation of surface plasmon wave (SPW) mechanisms has been considered as the most prominent scenario [25–31] for the ripple formation for femtosecond pulses, no previous investigation has addressed the possibility of suppression of electrodynamical mechanisms (i.e., suppression of SPW excitation) with increasing irradiation and how it could influence the surface profile of the material; hence a unified theoretical model that could provide a detailed description of the underlying fundamental physical processes for the entire range of structures is still elusive. To explain the laser-induced formation of such microstructures, a variety of complex mechanisms should therefore be explored, including electrodynamics, phase transitions, and molten material hydrodynamics as well as investigation of the role of viscous materials dynamics in determining the shape of the surface profile.

In this Rapid Communication, we present a theoretical model to account for the whole range of structures formed upon the interaction of a femtosecond laser beam with a conductive surface, shown for Si in Fig. 1. Specifically, the critical role of hydrodynamics on the femtosecond surface structuring process is elucidated. The developed theoretical model comprises [34] (i) an electromagnetics component that describes the surface plasmon wave excitation and interference with the incident beam that leads to a periodic modulation of the laser field energy density, (ii) a heat transfer component that accounts for carrier-lattice thermalization through particle dynamics and heat conduction and carrier-phonon coupling, and (iii) a hydrodynamics component that describes the molten material dynamics and resolidification process assuming an incompressible Newtonian fluid flow that includes recoil pressure and surface tension contributions [30] as well as Marangoni effects [35,36] and hydrothermal convection [37].

To predict the laser-induced morphological changes, simulations were performed with a p-polarized, Gaussian (both spatially and temporally) laser pulse of fluence $E_d = 0.7\,\mathrm{J/cm^2}$, pulse duration $\tau_p = 430\,\mathrm{fs}$, irradiation spot radius $R_0 = 15\,\mu\mathrm{m}$, and laser beam wavelength $\lambda = 800\,\mathrm{nm}$ [30]. A systematic analysis of the fundamental mechanism reveals that mass removal due to the fact that excessive temperatures are reached (larger than $\sim 0.90 T_c$, $T_c = 3540\,\mathrm{K}$) [38] and inhomogeneous deposition of the laser energy leads to recoil pressure, surface tension variance, and temperature gradients [Fig. 1(a) in Ref. [34]]. These effects induce a Marangoni-driven flow and capillary waves that eventually leads upon resolidification to the formation of a crater and a rippled profile

*tsibidis@iesl.forth.gr
†stratak@iesl.forth.gr

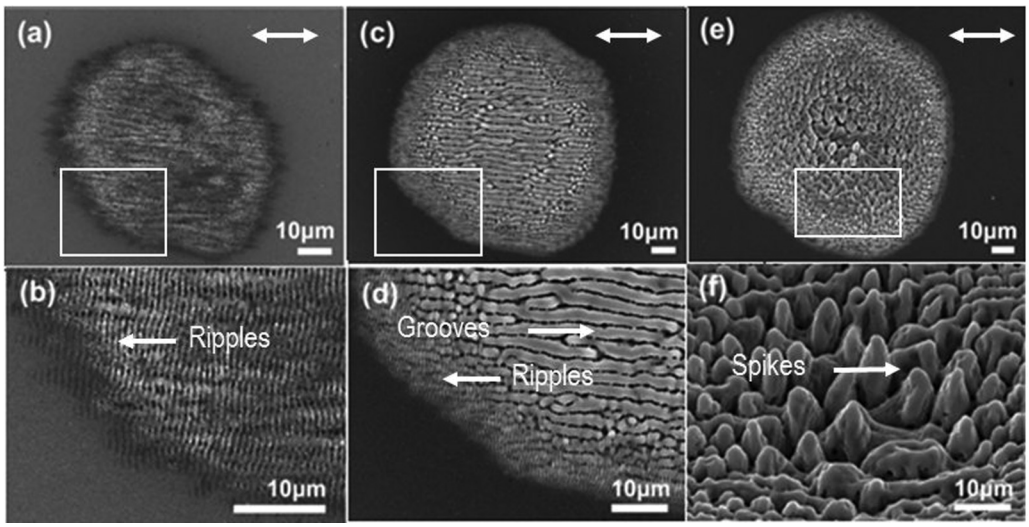

FIG. 1. Morphological changes induced on a Si surface following irradiation with NP = 10 (a), 40 (c), and 100 (e) pulses, where (b), (d), and (f) provide an enlarged area ($E_d = 0.7\,\mathrm{J/cm^2}$, $\tau_p = 430\,\mathrm{fs}$, $R_0 = 15\,\mu\mathrm{m}$). (Double-ended arrows indicate the laser beam polarization.)

while mass conservation and surface tension forces produce a protrusion near the periphery of the spot [Figs. 2(a) and 2(b) in Refs. [30,34]]. To evaluate the dependence of incubation effects with increasing number of pulses, the inhomogeneous energy deposition into the irradiated material is computed through the calculation of the product $\eta(\boldsymbol{k},\boldsymbol{k_i}) \times |b(\boldsymbol{k})|$ as

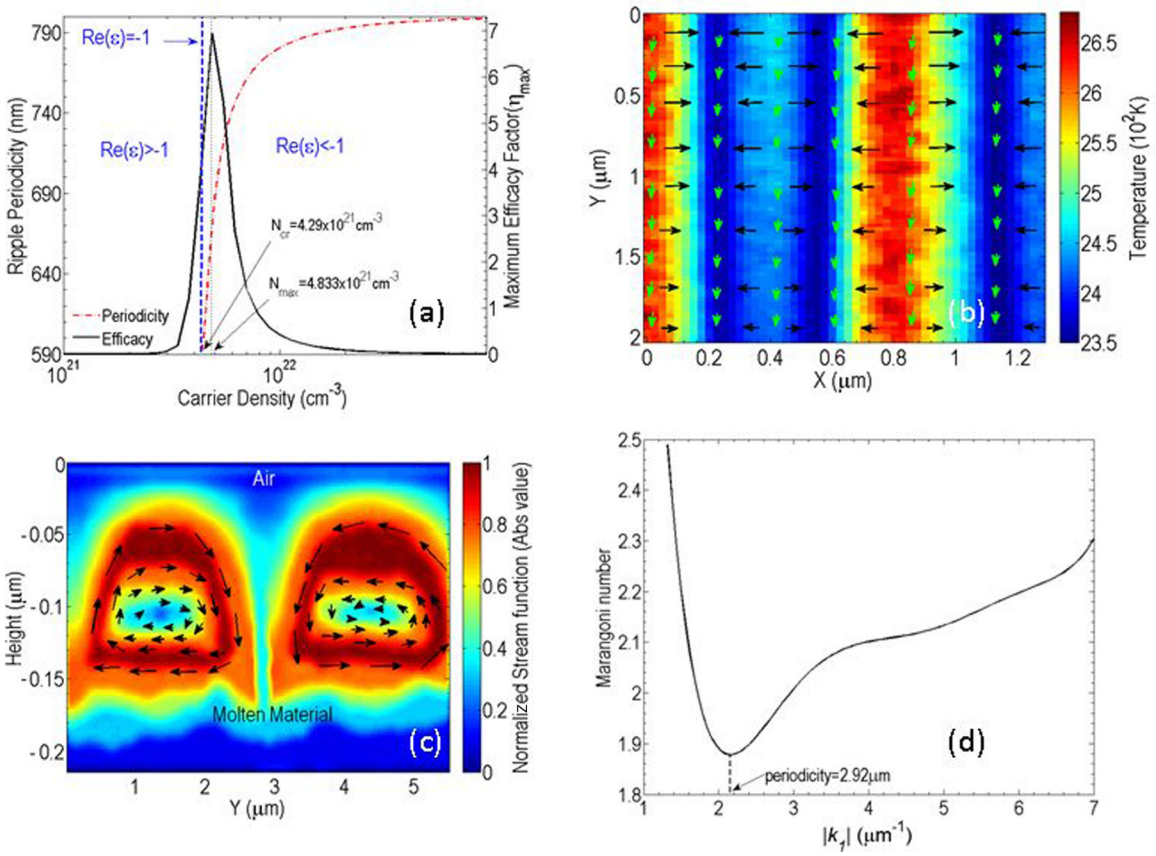

FIG. 2. (Color online) (a) Ripple periodicity dependence on the number of excited carriers (red *dotted* line). Maximum efficacy factor variation (for $s = 0.4$) with increasing density number is indicated by a *solid* line. Vertical blue and brown *dashed* lines indicate the condition for SPW excitation [$\mathrm{Re}(\varepsilon) \leftarrow 1$] and maximum $N_{\max}$, respectively. (b) Temperature field on the surface at $t = 1\,\mathrm{ns}$ (*black* and *green* arrows indicate the flow movement along the X, Y directions). (c) Stream function field at $t = 1\,\mathrm{ns}$ for NP = 20 along the Y axis (*black* arrows indicate the direction of the fluid movement considering the *absolute* value of the stream function [34] normalized to 1). (d) Marginal stability of the hydrothermal patterns for NP = 20 occurs at $|\boldsymbol{k}_1| = 2.1528\,\mu\mathrm{m}^{-1}$ (period $= 2.92\,\mu\mathrm{m}$) ($E_d = 0.7\,\mathrm{J/cm^2}$, $t_p = 430\,\mathrm{fs}$, $R_0 = 15\,\mu\mathrm{m}$).

described in the Sipe-Drude model [39,40]. In the above expression, η describes the efficacy with which the surface roughness at the wave vector $\boldsymbol{k}$ (i.e., $|\boldsymbol{k}| = 2\pi/\lambda$) induces inhomogeneous radiation absorption, $\boldsymbol{k_i}$ is the component of the wave vector of the incident beam on the material's surface plane and b represents a measure of the amplitude of the surface roughness at $\boldsymbol{k}$. The efficacy factor depends on the dielectric constant ε of the material [40] and therefore any variation of the carrier temperature and density due to inhomogeneous radiation absorption is expected to influence the dielectric constant, SPW, and finally ripple periodicity. Simulation results and experimental data [30] indicate the production of subwavelength-size ripples [Fig. 1(a) in Ref. [34]], which is consistent with previous experimental observations [7] and theoretical predictions [40].

To investigate morphological changes for a larger number of pulses, we notice that upon irradiation of the modified material with NP $\geqslant$ 20, a new type of laser-induced pattern is observed whose formation process has not been understood to date [Figs. 1(c) and 1(d)]. Interestingly, the produced structures exhibit a spatial periodicity which is higher than the ripples' wavelength (i.e., more than twice the laser wavelength). To explore the underlying physical mechanism that leads to the grooves formation, we first quantify the inhomogeneous energy deposition through the computation of the efficacy factor. This is presented in Fig. 2(a), showing the dependence of the ripples periodicity and the maximum efficacy factor on the carrier density. As can be seen, for carrier densities, ranging from $N_{\max} = 4.83 \times 10^{21}\,\mathrm{cm}^{-3}$ (i.e., where the efficacy factor attains maximum value) to $N_{cr} = 4.29 \times 10^{21}\,\mathrm{cm}^{-3}$ corresponding to the minimum value for SPW excitation [i.e., $\mathrm{Re}(\varepsilon) = -1$], the efficacy factor is decreasing which also leads to a decreasing inhomogeneous energy deposition [39,40]. On the other hand, for carrier densities higher than $N_{\max}$ an abrupt decrease and eventual vanishing of the efficacy factor occurs [25]. Furthermore, upon increasingly irradiating the material with more pulses, the surface relief deepens, characterized by an increasingly smaller shape factor s, which also leads to a rapidly decreasing efficacy factor [34]. The latter is nevertheless expected as energy absorption is influenced by the variations in the local angle of incidence and reflectivity. As a result, a gradual suppression of ripples would follow as the diminishing efficacy factor on the one hand leads to an amplitude decrease of the produced ripples, while the efficacy factor peak is reached at a level which is lower than the threshold of SPW excitation.

Ripples' suppression suggests that the origin of grooves cannot be ascribed to electrodynamics and SPW excitation; by contrast, a thorough investigation of the transient lattice temperature profile and the subsequent dynamic flow of the resulting molten material indicate that hydrodynamical effects are behind the grooves formation. We first elaborate on the dynamics of the molten material and analyze the melt resolidification process. More specifically, the rippled profile created for a low number of pulses constitutes a grating structure with a substantially larger surface modulation across the ripples [*black* arrows in Fig. 2(b)]. However, lateral fluid movement from both sides of the well [*blue* stripes in Fig. 2(b)] will hinder further material displacement. By contrast, the presence of a temperature gradient along the Y axis leads to surface stress that drives a shear flow, while the resulting temperature profile is capable of destabilizing the molten layer to Marangoni convection and production of hydrothermal waves perpendicularly to the thermal gradient [37]. This thermal-convective instability is indicative for fluids characterized by a low Prandtl number P_r [i.e., P_r (for molten Si) $= 0.017$ [34]] leading to transverse counter-rotating rolls [Fig. 2(c)] [34,37,41] in contrast to longitudinal convection rolls that occur for liquids with a high Prandtl number [37,42]. We hence postulate that when the temperature difference within the melt exceeds a critical value, convection rolls generated by surface tension gradients and hydrothermal waves will induce surface tractions, developed perpendicular to ripples orientation. In order to verify the above phenomenological description of the melt hydrodynamic flow and predict the generation of hydrothermal waves in thin liquid films through heat transfer and Marangoni convection, we solve Eqs. (7)–(12) and (17)–(23) in Ref. [34] and estimate the conditions that will lead to the formation of the aforementioned transverse structures [37,41–46]. In principle, the Marangoni number, M, that represents the ratio of the rate of convection and rate of conduction, is used to characterize the flow due to surface tension gradients through the relation $M = (\partial\sigma/\partial T)\Delta T\,\Delta H/(\alpha\mu)$, where $\partial\sigma/\partial T$, ΔT, ΔH, α, and μ are the surface tension gradient, average temperature difference between the lower and upper layer of the liquid, average thickness of the fluid, thermal diffusivity, and dynamic viscosity of the molten material, respectively. However, the fluid flow in a curved/inclined space and the spatiotemporal dependence of the rest of the parameters due to the highly nonlinear nature of the problem does not allow the derivation of a simple, analytic expression that provides a value for the onset of the roll movement, their stability conditions, and final profile upon solidification. Nevertheless, a numerical solution of the aforementioned equations is pursued using a finite difference methodology and a staggered grid [30] (see also, references therein) in which stress-free and no-slip (i.e., $\boldsymbol{u} = 0$) boundary conditions are imposed on the liquid-solid interface, while shear stress boundary conditions are assumed on the free surface. Using a common approach, the first step is to find equations describing the overall convective flow (i.e., base flow) followed by a linear stability analysis of small perturbations to the flow [47]. Then, the revised equations are solved using a semi-implicit time discretization fixing a wave vector $\boldsymbol{k_n} = [k_x(n), 0, k_z(n)]$ and seeking solutions in the form of normal modes for $u_{x,z}(\vec{r},t) \sim W(z)e^{-\omega t}\sum_n c_n e^{i\vec{k}_n\cdot\vec{r}}$, $T(\vec{r},t) \sim \theta(z)e^{-\omega t}\sum_n c_n e^{i\vec{k}_n\cdot\vec{r}}$, and $P(\vec{r},t) \sim p(z)e^{-\omega t}\sum_n c_n e^{i\vec{k}_n\cdot\vec{r}}$, for the velocity, temperature, and pressure, respectively, where $n = 1$ corresponds to the formation of transverse roll structures and $\omega(<0)$ is the growth rate of the structures. Based on the values of the hydrodynamic parameters and the temperature dependence of the physical parameters of liquid Si for NP $=$ 20, counter- rotating vortex rolls are formed which propagate perpendicularly to the molten material movement [Fig. 2(c)]. The molten flow is characterized by decreasing vorticity inside the roll, while the stream function at the bottom of the liquid indicates an almost parallel flow (that diminishes at larger depths) with shear [see also Fig. 4(b) in Ref. [34]]. Furthermore, the development of two rolls with opposite flow direction leads to a rapidly decreasing (i.e., close to stagnation) speed at the meeting point. To determine the stability of the

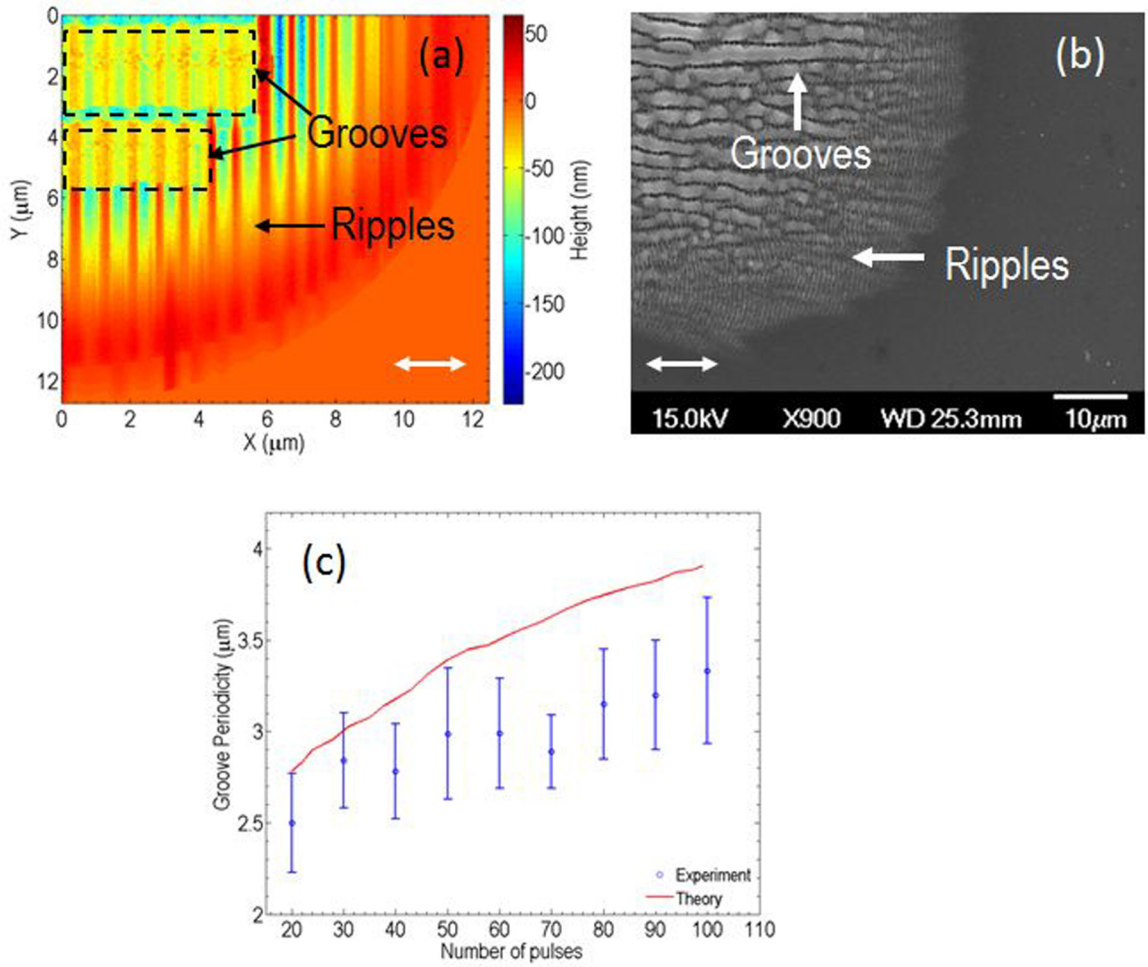

FIG. 3. (Color online) (a) Groove-ripple pattern for NP = 20. (b) Experimental results for NP = 20. (c) Groove periodicity vs number of pulses ($E_d = 0.7\,\mathrm{J/cm^2}$, $\tau_p = 430\,\mathrm{fs}$, $R_0 = 15\,\mu\mathrm{m}$). (Double-ended arrow indicates the laser beam polarization.)

roll patterns, we compute the (spatial) average Marangoni number as a function of $|\boldsymbol{k}_1|$ to estimate the critical value of the onset of convection which yields a periodicity equal to $|\boldsymbol{k}_i|/(2\pi) \sim 2.92\,\mu\mathrm{m}$ [Fig. 2(d)]. The graph suggests that the critical value of the Marangoni number $M_c \sim 1.88$ is the minimal value for which the molten layer is convectively unstable and leads to the formation of rolls with direction parallel to the ripples [46,47].

To predict the surface modification of the material following the fluid movement described above, we investigate the morphology attained when resolidification takes place for conditions that lead to $M_c \sim 1.88$. The resulting surface profile is illustrated in Fig. 3 (upper view) for NP = 20 with a groove periodicity equal to $\Lambda_{\mathrm{groove}} = 2.79\,\mu\mathrm{m}$ (i.e., resolidification process leads to the reduction of the groove periodicity compared to the roll structure wavelength of $2.92\,\mu\mathrm{m}$); it is obvious that three types of structures are produced at the same time: (i) conventional ripples with a subwavelength periodicity in the spot area where the criteria for SPW excitation are fulfilled, (ii) grooves (area enclosed in *dashed* lines) with periodicity of $\sim\Lambda_{\mathrm{groove}}$, and (iii) pseudoripples (to distinguish them from the conventional ripples) appearing on top of the grooves as well as in the spaces among them and they are remains of the ripples formed at low NPs (see Ref. [34]). Therefore the amplitude of the capillary waves created due to Marangoni convection is not large enough to eliminate the ripple profile leading to the formation of pseudoripples. An experimental validation of the grooves and ripples coexistence and their relative unequal periodicities is illustrated in Fig. 3(b). While the pseudoripples do not appear in this case, unlike theoretical results [Fig. 3(a)], experiments performed on metal surfaces (i.e., titanium [34]) show that the presence of such structures is possible and the presented scenario could reveal the critical role of hydrodynamic instabilities on surface patterning. Numerical simulations indicate that the height of the pseudoripples decreases with increasing NP due to the increase of the volume of the elevated molten material leading to progressive suppression of capillary wave amplitude [34]. Further analysis was also conducted to investigate grooves' periodicity dependence on the number of pulses ($100 \geqslant \mathrm{NP} \geqslant 20$). Upon increasing NP, the enhanced mass removal and deepening of the surface profile causes enhanced energy deposition and temperature gradients. As a result, an increased outward movement of the molten is produced. Accordingly, simulation results predict that as NP increases hydrothermal rolls with an increasing periodicity pattern are produced. Hence, the proposed model predicts that the groove periodicity is an increasing function of the number of pulses,

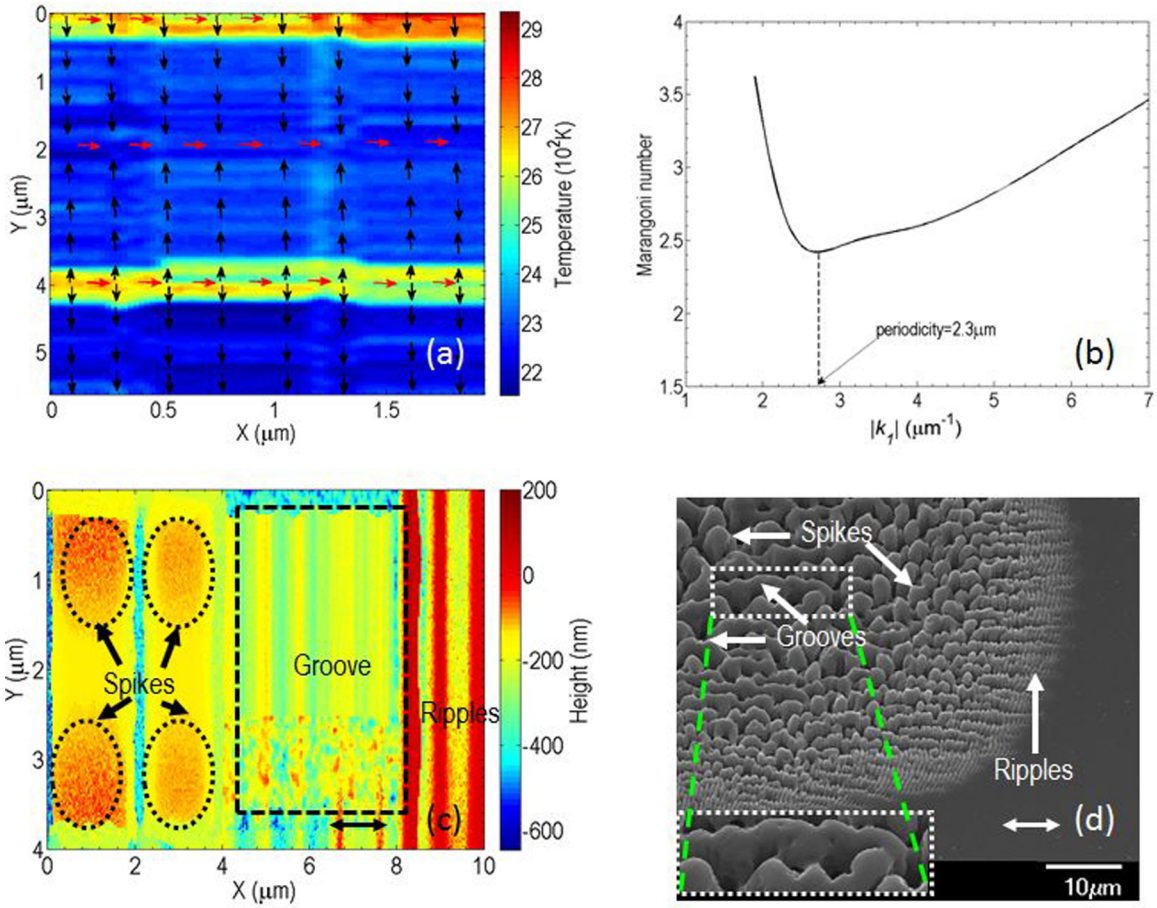

FIG. 4. (Color online) (a) Temperature field on the surface at $t = 1$ ns for NP = 120 (*black* and *red* arrows indicate the flow movement along the X and Y directions, while the *blue* region characterizes the area occupied by the groove). (b) Stability of the convection roll patterns for $NP = 120$ occurs at $|\boldsymbol{k}_1| = 2.7318\,\mu\text{m}^{-1}$ (period $= 2.3\,\mu$m). (c) Surface pattern for NP = 120 (encircled objects are hills and groove is enclosed in the boxed area). (d) Experimental results for NP = 200 ($E_d = 0.7\,\text{J/cm}^2$, $\tau_p = 430$ fs, $R_0 = 15\,\mu$m). (Double-ended arrow indicates the laser beam polarization.)

which is similar to the trend observed in the experiments [Fig. 3(c)].

To explore whether the gradual diminishing of the pseudoripples and increase of grooves periodicity further influences the melt flow and the resulting profile, we performed simulations at higher number of pulses, i.e., NP $\geqslant$ 100. The disappearance of pseudoripples combined with the enhanced temperature gradients generated from the grooves' grating in this case drives predominantly the fluid flow in a direction perpendicularly to the laser beam polarization vector [Fig. 4(a)]. Hence, surface tension gradients and temperature differences will produce an overall preferred Marangoni convection along the X axis and thus hydrothermal waves will be induced, following a similar process to the one described previously for grooves formation (however, the rolls are currently developed in the opposite direction). In particular, base flow with a subsequent linear analysis procedure is followed for a wave vector $\boldsymbol{k}_n = [0, k_y(n), k_z(n)]$, while the onset for the development of roll structures occurs on top of the original (i.e., along the X axis) grooves when the wavelength of the periodical modulation is $\sim$2.3 μm corresponding to a Marangoni number equal to $M_c \sim 2.4$ [Fig. 4(b)]. Notably, the roll patterns due to the convective instability evolve into protruding structures with a periodicity of $\Lambda_{\text{protruded}} = 2.1\,\mu$m upon melt solidification. The height of the protruding structures progressively increases with increasing the number of pulses giving rise to spikelike assemblies upon further irradiation [Fig. 4(c) encircled objects] [34]. The simulation predictions presented above show remarkable similarity with the surface morphology obtained from experiments performed at identical irradiation conditions, while the produced hills can be viewed as the precursors of microspikes. This is evident in Fig. 4(d), where the coexistence of grooves and microspikes can be observed. Moreover, it is obvious that the grooves' profile is spatially modulated and the corrugation wavelength is of the size of the grooves' periodicity ($\geqslant$2.1 μm). The similarities between our theoretical model and experimental findings [Figs. 4(c) and 4(d)], especially concerning the predicted periodicities, could work towards formulating a comprehensive theoretical framework that accounts for the formation of these structures. Although further investigation is required to establish a more enlightening picture of the process of microgrooves and spikes formation, it is evident that the proposed model underlines conclusively the predominant role of hydrodynamical processes.

In summary, the physical mechanism that accounts for the various stages of the structuring process taking place

upon irradiation of a conductive solid with multiple identical femtosecond laser pulses has been demonstrated. In particular, a hybrid model is proposed based on melt hydrodynamics complemented with electromagnetic interference effects to account for ripples, while Marangoni shear generated convection dominates the mechanism that leads to hydrothermal waves and eventually to microgrooves and microspikes formation. The proposed interpretation can first enhance our understanding of the fundamental physical processes that characterize ultrashort laser-matter interaction, and secondly allow control of the optoelectronic characteristics of the different structures, which is expected to meet a wide range of applications in industry and biomedicine.

The authors acknowledge financial support from the "3DNeuroscaffolds" and "SolarNano" projects. This work was also partly supported by the Integrated Initiative of European Laser Research Infrastructures LASERLAB-III (Grant Agreement No. 2012-284464).

[1] S. K. Sundaram and E. Mazur, Nat. Mater. **1**, 217 (2002).
[2] A. Y. Vorobyev and C. Guo, Laser Photonics Rev. **7**, 385 (2012).
[3] E. Stratakis, Sci. Adv. Mater. **4**, 407 (2012).
[4] V. Zorba, L. Persano, D. Pisignano, A. Athanassiou, E. Stratakis, R. Cingolani, P. Tzanetakis, and C. Fotakis, Nanotechnology **17**, 3234 (2006).
[5] H. M. van Driel, Phys. Rev. B **35**, 8166 (1987).
[6] E. Knoesel, A. Hotzel, and M. Wolf, Phys. Rev. B **57**, 12812 (1998).
[7] Y. H. Han and S. L. Qu, Chem. Phys. Lett. **495**, 241 (2010).
[8] T. H. Her, R. J. Finlay, C. Wu, S. Deliwala, and E. Mazur, Appl. Phys. Lett. **73**, 1673 (1998).
[9] A. J. Pedraza, J. D. Fowlkes, and Y. F. Guan, Appl. Phys. A **77**, 277 (2003).
[10] V. Bergeron, C. Berger, and M. D. Betterton, Phys. Rev. Lett. **96**, 098502 (2006).
[11] N. A. Maximenko, O. V. Melnichenko, P. P. Niiler, and H. Sasaki, Geophys. Res. Lett. **35**, 08603 (2008).
[12] R. W. Griffiths, R. C. Kerr, and K. V. Cashman, J. Fluid Mech. **496**, 33 (2003).
[13] D. S. Ivanov and L. V. Zhigilei, Phys. Rev. B **68**, 064114 (2003).
[14] M. E. Povarnitsyn, T. E. Itina, M. Sentis, K. V. Khishchenko, and P. R. Levashov, Phys. Rev. B **75**, 235414 (2007).
[15] N. M. Bulgakova, I. M. Bourakov, and N. A. Bulgakova, Phys. Rev. E **63**, 046311 (2001).
[16] J. P. Colombier, P. Combis, F. Bonneau, R. Le Harzic, and E. Audouard, Phys. Rev. B **71**, 165406 (2005).
[17] R. Cuerno, H. A. Makse, S. Tomassone, S. T. Harrington, and H. E. Stanley, Phys. Rev. Lett. **75**, 4464 (1995).
[18] C. P. Grigoropoulos, H. K. Park, and X. Xu, Int. J. Heat Mass Transf. **36**, 919 (1993).
[19] E. G. Gamaly, S. Juodkazis, K. Nishimura, H. Misawa, B. Luther-Davies, L. Hallo, P. Nicolai, and V. T. Tikhonchuk, Phys. Rev. B **73**, 214101 (2006).
[20] J. Godet, L. Pizzagalli, S. Brochard, and P. Beauchamp, Phys. Rev. B **70**, 054109 (2004).
[21] W. Q. Hu, Y. C. Shin, and G. King, Phys. Rev. B **82**, 094111 (2010).
[22] J. A. Sanchez and M. P. Menguc, Phys. Rev. B **76**, 224104 (2007).
[23] M. E. Povarnitsyn, T. E. Itina, K. V. Khishchenko, and P. R. Levashov, Phys. Rev. Lett. **103**, 195002 (2009).
[24] N. A. Kirichenko, Quantum Electron. **39**, 442 (2009).
[25] J. Bonse, A. Rosenfeld, and J. Kruger, J. Appl. Phys. **106**, 104910 (2009).
[26] M. Huang, F. L. Zhao, Y. Cheng, N. S. Xu, and Z. Z. Xu, ACS Nano **3**, 4062 (2009).
[27] T. J. Y. Derrien, T. E. Itina, R. Torres, T. Sarnet, and M. Sentis, J. Appl. Phys. **114**, 083104 (2013).
[28] O. Varlamova, F. Costache, M. Ratzke, and J. Reif, Appl. Surf. Sci. **253**, 7932 (2007).
[29] M. Barberoglou, G. D. Tsibidis, D. Gray, E. Magoulakis, C. Fotakis, E. Stratakis, and P. A. Loukakos, Appl. Phys. A **113**, 273 (2013).
[30] G. D. Tsibidis, M. Barberoglou, P. A. Loukakos, E. Stratakis, and C. Fotakis, Phys. Rev. B **86**, 115316 (2012).
[31] G. D. Tsibidis, E. Stratakis, and K. E. Aifantis, J. Appl. Phys. **111**, 053502 (2012).
[32] A. Y. Vorobyev and C. Guo, J. Appl. Phys. **104**, 063523 (2008).
[33] S. I. Dolgaev, N. A. Kirichenko, A. V. Simakin, and G. A. Shafeev, Appl. Surf. Sci. **253**, 7987 (2007).
[34] See Supplemental Material at http://link.aps.org/supplemental/10.1103/PhysRevB.92.041405 for a detailed discussion of the model and simulation results.
[35] L. E. Scriven and C. V. Sternling, Nature (London) **187**, 186 (1960).
[36] J. Svensson, N. M. Bulgakova, O. A. Nerushev, and E. E. B. Campbell, Phys. Rev. B **73**, 205413 (2006).
[37] M. K. Smith and S. H. Davis, J. Fluid Mech. **132**, 119 (1983).
[38] R. Kelly and A. Miotello, Appl. Surf. Sci. **96–98**, 205 (1996).
[39] J. Bonse, M. Munz, and H. Sturm, J. Appl. Phys. **97**, 013538 (2005).
[40] J. E. Sipe, J. F. Young, J. S. Preston, and H. M. van Driel, Phys. Rev. B **27**, 1141 (1983).
[41] A. E. Hosoi and J. W. M. Bush, J. Fluid Mech. **442**, 217 (2001).
[42] J. R. A. Pearson, J. Fluid Mech. **4**, 489 (1958).
[43] A. Alexeev, T. Gambaryan-Roisman, and P. Stephan, Phys. Fluids **17**, 062106 (2005).
[44] F. H. Busse, J. Fluid Mech. **52**, 97 (1972).
[45] I. M. R. Sadiq, R. Usha, and S. W. Joo, Chem. Eng. Sci. **65**, 4443 (2010).
[46] Y. Mori and Y. Uchida, Int. J. Heat Mass Transf. **9**, 803 (1966).
[47] F. H. Busse, Rep. Prog. Phys. **41**, 1929 (1978).